

# Moist-convective thermal rotating shallow water model

Cite as: Phys. Fluids **32**, 066601 (2020); <https://doi.org/10.1063/5.0007757>

Submitted: 16 March 2020 . Accepted: 12 May 2020 . Published Online: 01 June 2020

Alexander Kurganov, Yongle Liu , and Vladimir Zeitlin



View Online



Export Citation




CrossMark



**NEW!**

Sign up for topic alerts  
New articles delivered to your inbox



# Moist-convective thermal rotating shallow water model

Cite as: *Phys. Fluids* **32**, 066601 (2020); doi: [10.1063/5.0007757](https://doi.org/10.1063/5.0007757)

Submitted: 16 March 2020 • Accepted: 12 May 2020 •

Published Online: 1 June 2020



View Online



Export Citation



CrossMark

Alexander Kurganov,<sup>1,2</sup> Yongle Liu,<sup>1,3,a)</sup>  and Vladimir Zeitlin<sup>1,4</sup>

## AFFILIATIONS

<sup>1</sup>Department of Mathematics, Southern University of Science and Technology, Shenzhen 518055, China

<sup>2</sup>SUSTech International Center for Mathematics, Southern University of Science and Technology, Shenzhen 518055, China

<sup>3</sup>Department of Mathematics, Harbin Institute of Technology, Harbin 150001, China

<sup>4</sup>Laboratory of Dynamical Meteorology, Sorbonne University, Ecole Normale Supérieure, CNRS, 24 rue Lhomond, 75005 Paris, France

<sup>a)</sup> Author to whom correspondence should be addressed: [liuyl2017@mail.sustech.edu.cn](mailto:liuyl2017@mail.sustech.edu.cn)

## ABSTRACT

We show how the moist-convective rotating shallow water model, where the moist convection and the related latent heat release are incorporated into the standard rotating shallow water model of the atmosphere, can be improved by introducing, in a self-consistent way, horizontal gradients of potential temperature and changes of the latter due to the condensation heating, radiative cooling, and ocean-atmosphere heat fluxes. We also construct the quasi-geostrophic limit of the model in mid-latitudes and its weak-gradient limits in the equatorial region. The capabilities of the new model are illustrated by the examples of convection-coupled gravity waves and equatorial waves produced by the relaxation of localized pressure and potential temperature anomalies in the presence of moist convection.

Published under license by AIP Publishing. <https://doi.org/10.1063/5.0007757>

## I. INTRODUCTION

Simplified models, which are obtained by space and/or time averaging of the full “primitive” equations, are the standard conceptual tools for understanding fundamental dynamical processes in the atmosphere. Among them, the rotating shallow water (RSW) model plays a distinguished role. The history of applications of this model and of its reduction to slow motions, the barotropic quasi-geostrophic (QG) model, is long, and the examples of applications are numerous; see, e.g., Ref. 1. Let us just mention that the dynamics of the equatorial atmosphere was first theoretically understood using this model in Ref. 2. Yet, in its classical version, the RSW model misses an essential ingredient: phase transitions of water vapor with the related latent heat release and their influence upon dynamical processes. The moist-convective rotating shallow water (mcRSW) model was introduced in Ref. 3 in the one-layer configuration and then extended to two layers in Ref. 4 in order to repair this drawback of the original RSW model. It incorporates the bulk, vertically averaged, effects of condensation and the related heat release upon the air column in a simple albeit consistent way, and allows us to study

the dynamical influence of moist convection by analytically simple and numerically friendly means. The model is a natural extension of the seminal ideas of Ref. 5 and was shown to capture the essential properties of moist barotropic and baroclinic instabilities of jets<sup>6,7</sup> and vortices,<sup>8</sup> including the instabilities of intense hurricane-type ones.<sup>9,10</sup> The model can be extended to include, together with the water vapor, liquid water, vaporization, and precipitation.<sup>10</sup> Despite these achievements, there is an essential ingredient that is lacking in the model. As its parent model, the RSW equations, it does not allow for horizontal variations of the potential temperature. This is why, for example, in the mcRSW model, the latent heat release is associated uniquely with the convective mass flux. Yet, there exists in the literature a variant of the shallow water model with horizontal density and/or temperature gradients, the so-called thermal rotating shallow water (TRSW) equations; see, e.g., Ref. 11. The TRSW equations were multiply reinvented both in the meteorological and in the oceanographic literature, in the context of the boundary layer in the atmosphere<sup>12,13</sup> and of the mixed layer in the ocean<sup>14–16</sup> (the model is sometimes called the Ripa system). A natural idea, thus, arises to include the bulk moisture and to apply the simple parameterization

of the moist convection, which is used in mcRSW, not in RSW but in TRSW. It seems natural to associate, then, the latent heat release with an increase in the mean potential temperature and not with a convective mass flux. This idea was formulated in Ref. 3, but not pursued, as it was shown to lead to physically inconsistent relationship between the phase velocities of moist and dry gravity waves. At the same time, a possibility was mentioned in Ref. 3 to split the influence of the latent heat release into two parts: heating, that is, local increase of potential temperature, and convective flux. Below we will show that this idea can be successfully realized, leading to a consistent moist-convective TRSW (mcTRSW) model with an improved representation of thermodynamic processes, when compared to the mcRSW model.

The main advantage of the mcTRSW model is that it allows us to account for both mechanical and thermal effects of the moist convection and, thus, can be used to improve the TRSW modeling of various dynamical phenomena in the atmosphere, the most important being convection-coupled waves and vortices.

The paper is organized as follows: In Sec. II, we construct the basic “skeleton” version of the mcTRSW model from the first principles, determine the admissible values of parameters by analyzing its wave spectrum, formulate and analyze the asymptotic limits of the model, and finally, add more physics by including parameterized interactions with the boundary layer and outer atmosphere. In Sec. III, we give examples of the applications of the model. We, first, benchmark it by corresponding constant-temperature simulations, then simulate the propagation of convection-coupled gravity waves and evolution (adjustment) of localized pressure and temperature perturbations at the Equator. The Appendix contains a sketch of the numerical scheme.

## II. CONSTRUCTING THE mcTRSW MODEL

### A. The “skeleton” version of the mcTRSW equations

We first recall the equations of the one-layer TRSW model in the absence of dissipation on the beta-plane. They are written for the horizontal velocity  $\mathbf{v}(x, y, t) = (u(x, y, t), v(x, y, t))^T$ , thickness  $h(x, y, t)$ , and the field  $b(x, y, t)$  that represents the temperature/density variations:

$$\mathbf{v}_t + \mathbf{v} \cdot \nabla \mathbf{v} + f(y) \hat{z} \wedge \mathbf{v} = -b \nabla h - \frac{h}{2} \nabla b, \quad (1a)$$

$$h_t + \nabla \cdot (h \mathbf{v}) = 0, \quad (1b)$$

$$b_t + \mathbf{v} \cdot \nabla b = 0. \quad (1c)$$

Here,  $\nabla = (\partial/\partial x, \partial/\partial y)$ ,  $\hat{z}$  is the unit vector in the vertical direction, and  $f(y) = f_0 + \beta y$  is the Coriolis parameter with  $f_0$  and  $\beta$  being non-negative constants. Here and below, we use index notation for the corresponding partial derivatives if it does not lead to any confusion. In the atmospheric context, the model can be derived by vertical-averaging between a pair of material surfaces of the primitive equations with the pseudo-height as a vertical coordinate, applying the mean-field hypothesis and relaxing the standard in derivation of the shallow water model assumption of the horizontal homogeneity of potential temperature (Ref. 1, Chap. 14). The variable  $b$ , then, has a

meaning of buoyancy in terms of vertically averaged potential temperature (see Ref. 3):  $b = g\theta(x, y, t)/\theta_0$ , where  $\theta(x, y, t)$  is the variable part and  $\theta_0$  is a reference value for the potential temperature, and  $b$  has the same dimensions as  $g$ ,  $m/s^2$ . We recall that the “dry” potential temperature is, up to a constant, the exponential of entropy. The variable  $h$  has a meaning of geopotential thickness [geopotential height in the absence of bottom topography, and the latter can be easily added by replacing  $h$  with  $h + Z(x, y)$  in the first term on the right-hand side (RHS) of (1a)]. The bulk humidity (vertically integrated specific humidity)  $Q$  is a passive tracer in the absence of condensation, obeying the equation

$$Q_t + \nabla \cdot (Q \mathbf{v}) = 0. \quad (2)$$

The mass of the water vapor is neglected in the mass conservation Eq. (1b).

Let us construct the basic version of the mcTRSW equations, which we will then ameliorate. By applying the same philosophy as in Ref. 3, we consider that when the bulk humidity exceeds a saturation threshold, the condensation starts, providing a sink in (2). With a relaxation parameterization for the condensation, Eq. (2) becomes

$$Q_t + \nabla \cdot (Q \mathbf{v}) = -C := -\frac{Q - Q_s}{\tau} \mathcal{H}(Q - Q_s), \quad (3)$$

where  $\mathcal{H}$  denotes the Heaviside function and  $\tau$  is relaxation time. In the simplest version of the model, the saturation threshold  $Q_s$  can be taken to be constant, although a dependence of  $Q_s$  on  $h$  is easy to add, as well as now, when  $\theta$  can vary, a dependence on  $\theta$ . Both could be reasonably taken to be linear as in Ref. 3. The relaxation time is short in the atmosphere, of the order of a couple of hours. An important limit, therefore, is that of immediate relaxation (see Ref. 5),

$$\tau \rightarrow 0; \quad C \rightarrow -Q_s \nabla \cdot \mathbf{v}. \quad (4)$$

The condensation leads to the latent heat release, which is associated in the mcTRSW model with a sink in Eq. (1b) due to the resulting convective flux,

$$h_t + \nabla \cdot (h \mathbf{v}) = -\beta_1 C, \quad (5)$$

where the coefficient  $\beta_1$  was determined in Ref. 3 with the help of a vertically averaged equation of Lagrangian conservation of the linearized equivalent potential temperature (which was called moist enthalpy in Ref. 3). In the TRSW model with variable potential temperature, the heating due to condensation should increase the entropy, and hence the potential temperature, which should acquire, thus, a source,

$$b_t + \mathbf{v} \cdot \nabla b = \beta_2 C, \quad (6)$$

where  $\beta_2$  is another coefficient. Combining Eqs. (1a), (5), (6), and (3), we obtain the simplest “skeleton” version of the mcTRSW equations. The coefficients  $\beta_1$  and  $\beta_2$  are not determined yet and can, in principle, depend on the dynamical variables, which will be the case as we show later. Notice that Eqs. (5) and (6) can be combined to give

$$(hb)_t + \nabla \cdot (\mathbf{v}bh) = (\beta_2 h - \beta_1 b)C, \quad (7)$$

which expresses the evolution of the bulk (vertically integrated) potential temperature and hence of the bulk entropy of the air column. A natural physical constraint on the values of the coefficients

$\beta_1$  and  $\beta_2$  is, thus, the non-negativity of the RHS of (7). Another constraint (see Ref. 3) is that of higher phase velocities of dry, as compared to moist, gravity waves, which follows from the observations. In order to analyze this constraint, let us take, for simplicity, the one-dimensional (1-D) moist-convective thermal shallow water without rotation (a schematic representation of this model is presented in Fig. 1),

$$\begin{cases} u_t + uu_x = -bh_x - \frac{b_x}{2}h, \\ h_t + (hu)_x = -\beta_1 C, \\ b_t + ub_x = \beta_2 C, \\ Q_t + (Qu)_x = -C, \end{cases} \quad (8)$$

and consider it in the limit of immediate relaxation  $C = -u_x Q_s$  with constant  $Q_s$ ; see (4). Linearizing (8) about the state of rest with uniform thickness  $H$  and buoyancy  $B-h = H + \eta$  and  $b = B + \sigma$ —and assuming  $\beta_1$  and  $\beta_2$  to be constant, we obtain a system describing moist (that is, convection-coupled) gravity waves,

$$\begin{cases} u_t + B\eta_x + \frac{H}{2}\sigma_x = 0, \\ \eta_t + (H - \beta_1 Q_s)u_x = 0, \\ \sigma_t + \beta_2 Q_s u_x = 0, \end{cases} \quad (9)$$

which can be readily reduced into a single wave equation,

$$u_{tt} - \left[ BH - \left( \beta_1 B - \beta_2 \frac{H}{2} \right) Q_s \right] u_{xx} = 0,$$

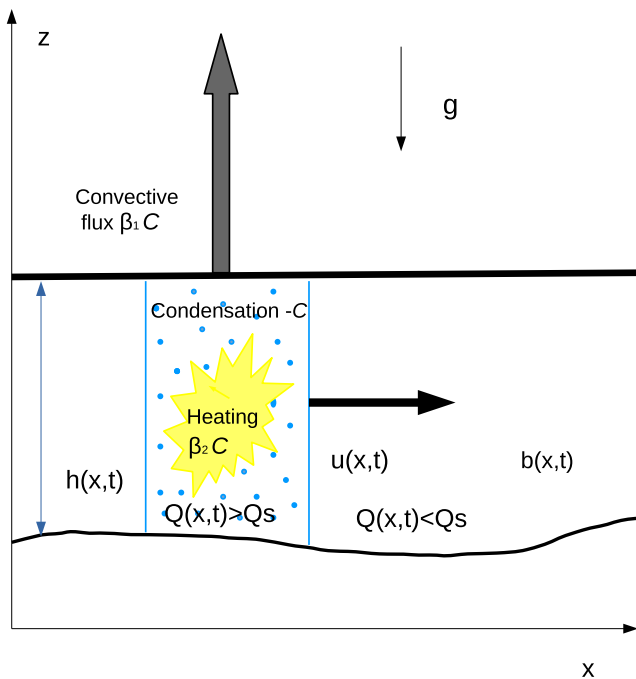


FIG. 1. A sketch of 1-D moist-convective shallow water model.

giving the following phase velocities of the moist waves:

$$c_m = \pm \sqrt{BH - \left( \beta_1 B - \beta_2 \frac{H}{2} \right) Q_s}. \quad (10)$$

The phase velocities of the dry waves are, obviously,  $c_d = \pm \sqrt{BH}$ . Hence, in order to satisfy the condition of non-decrease of the overall entropy in the layer and the condition that dry waves are faster than moist ones, the coefficients  $\beta_1$  and  $\beta_2$ , and the mean thickness  $H$  and buoyancy  $B$ , should satisfy the following inequalities:

$$\beta_1 B \leq \beta_2 H < 2\beta_1 B. \quad (11)$$

We note that the configuration where entropy is overall conserved, which is mentioned in Ref. 3, corresponds to  $\beta_1 B = \beta_2 H$  and is included in (11).

Let us now exploit the Lagrangian conservation of the linearized equivalent potential temperature (moist enthalpy). In the full three-dimensional (3-D) primitive equations, it reads

$$\frac{d}{dt} \left( \theta + \frac{L}{c_p} q \right) = 0, \quad (12)$$

where  $d/dt := \partial/\partial t + \mathbf{u} \cdot \nabla$  stands for the 3-D Lagrangian (material or advective) derivative with the 3-D velocity  $\mathbf{u} = (u, v, w)^\top$ ,  $\theta(x, y, z, t)$  is the potential temperature,  $q(x, y, z, t)$  is (non-dimensional) specific humidity,  $L$  is the specific heat of vaporization, and  $c_p$  is the specific heat at constant pressure. Following Ref. 3 and integrating (12) in  $z$  between a pair of material surfaces  $z = z_1(x, y, t)$  and  $z = z_2(x, y, t)$ , such that  $h = z_2 - z_1$ , which, by definition, are moving with the vertical velocities of the fluid  $w_1 = dz_1/dt$  and  $w_2 = dz_2/dt$ , we obtain

$$\Delta[\bar{\theta}h] + \frac{L}{c_p} \Delta[Q] + \mathcal{F} \left( \theta(z_2) + \frac{L}{c_p} q(z_2) \right) = 0,$$

where  $\mathcal{F}$  denotes a convective flux across  $z_2$ , and we have used the same notation as in Ref. 3:  $\Delta(\cdot) := (\cdot)_t + \nabla \cdot (\bar{\mathbf{v}}(\cdot))$ , where  $\bar{\mathbf{v}} = (\bar{u}, \bar{v})^\top$  is the vertically averaged horizontal velocity in the layer, and  $\bar{\theta}$  denotes the vertically averaged potential temperature. By the definition of the convective flux, it is a mass sink. Hence,  $\mathcal{F} = -\Delta[h]$ , and we obtain

$$\Delta[\bar{\theta}h] + \frac{L}{c_p} \Delta[Q] - \Delta[h] \left( \theta(z_2) + \frac{L}{c_p} q(z_2) \right) = 0, \quad (13)$$

where, by construction,  $\Delta[Q] = -C$  is to be substituted in (13). Notice that the potential temperature and moisture calculated at the upper surface in (13) can be approximated by their averages in the layer values  $\bar{\theta}, \bar{q}$ . Also notice that the coefficient  $L/c_p$  can be absorbed in  $q$ , and hence in  $Q$  and  $C$ , leading just to a renormalization of the relaxation time in the latter, which will be understood in what follows.

Contrary to the case of constant  $\bar{\theta}$  treated in Ref. 3,  $\Delta[h]$  cannot be unambiguously determined from (13) in terms of  $C$ , and some additional hypothesis is needed. As already discussed, a natural one is that of increase of  $\bar{\theta}h \equiv \int_{z_1}^{z_2} \theta dz$  due to the latent heat release produced by condensation:

$$\Delta[\bar{\theta}h] = \gamma C, \quad (14)$$

where  $\gamma > 0$  is a parameter. Substituting (14) in (13), and omitting from now on the bars over the vertically averaged quantities results in

$$\Delta[h] = -\frac{1-\gamma}{\theta+q} C, \quad (15)$$

where we have absorbed  $L/c_p$  in the humidity, as explained. From (14) and (15), we obtain

$$\frac{d_2}{dt} \theta \equiv \left( \frac{\partial}{\partial t} + \mathbf{v} \cdot \nabla \right) \theta = \frac{1}{h} \frac{\theta + \gamma q}{\theta + q} C, \quad (16)$$

where  $d_2/dt$  stands for the advective (Lagrangian) derivative with the vertically averaged horizontal velocity  $\mathbf{v}$ .

Let us now recall that the use of the linearized form  $\theta + Lq/c_p$  of the equivalent potential temperature in (12) is based on the smallness of the second term compared to the first, which corresponds to the physical reality. Hence, we can neglect the moisture terms in the first approximation in (15) and (16), and thus obtain the simplified expressions

$$\Delta[h] = -\frac{1-\gamma}{\theta} C, \quad \frac{d_2}{dt} \theta = \frac{1}{h} C. \quad (17)$$

Thus, in this approximation

$$\beta_1 = \frac{g}{\theta_0} \frac{1-\gamma}{b}, \quad \beta_2 = \frac{g}{\theta_0} \frac{1}{h}, \quad (18)$$

and it follows from (11) that the only constraint to impose on the value of the parameter  $\gamma$  is  $0 \leq \gamma < 1/2$ . Corrections to the expressions (17) following from (15) and (16) can be added, if necessary.

Thus, with  $\beta_1$  and  $\beta_2$  obeying (18), the equations of the “skeleton” mcTRSW model read as

$$\mathbf{v}_t + \mathbf{v} \cdot \nabla \mathbf{v} + f(y) \hat{z} \wedge \mathbf{v} = -b \nabla h - \frac{h}{2} \nabla b, \quad (19a)$$

$$h_t + \nabla \cdot (h \mathbf{v}) = -\frac{1-\gamma}{b} \frac{Q - Q_s}{\tau} \mathcal{H}(Q - Q_s), \quad (19b)$$

$$b_t + \mathbf{v} \cdot \nabla b = \frac{1}{h} \frac{Q - Q_s}{\tau} \mathcal{H}(Q - Q_s), \quad (19c)$$

$$Q_t + \nabla \cdot (Q \mathbf{v}) = -\frac{Q - Q_s}{\tau} \mathcal{H}(Q - Q_s), \quad (19d)$$

where we have absorbed the factor  $g/\theta_0$  in  $\beta_1$  and  $\beta_2$  in (18) in the bulk humidity  $Q$ , which, taking into account the previous renormalization, thus acquires the same dimensions as the product  $BH$ , that is,  $m^2/s^2$ .

## B. Asymptotic limits

### 1. Quasi-geostrophic (QG) limit on the $f$ -plane

Let us recall that the quasi-geostrophic (QG) limit of the “dry” TRSW model<sup>11</sup> is obtained with the following scaling:

$$u \sim U, \quad v \sim U, \quad x \sim L, \quad y \sim L, \quad t \sim \frac{L}{U} \quad (20)$$

and the hypotheses that deviations of thickness and buoyancy from their mean values are small and are of the same order as the Rossby number  $Ro = U/f_0 L \equiv \varepsilon$ , which gives

$$h(x, y, t) = H(1 + \varepsilon \eta(x, y, t)), \quad b(x, y, t) = B(1 + 2\varepsilon \sigma(x, y, t)). \quad (21)$$

As usual in the QG approximation, we suppose that the Burger number  $Bu = BH/f_0^2 L^2$  is of order one. Under this scaling, the system (IIA) becomes

$$\varepsilon(\mathbf{v}_t + \mathbf{v} \cdot \nabla \mathbf{v}) + \hat{z} \wedge \mathbf{v} = -(1 + 2\varepsilon \sigma) \nabla \eta - (1 + \varepsilon \eta) \nabla \sigma, \quad (22a)$$

$$\varepsilon \eta_t + \nabla \cdot ((1 + \varepsilon \eta) \mathbf{v}) = -\frac{1-\gamma}{(1 + 2\varepsilon \sigma)} \bar{C}, \quad (22b)$$

$$\sigma_t + \mathbf{v} \cdot \nabla \sigma = \frac{1}{2\varepsilon(1 + \varepsilon \eta)} \bar{C}, \quad (22c)$$

$$\bar{Q}_t + \nabla \cdot (\bar{Q} \mathbf{v}) = -\bar{C}, \quad (22d)$$

where  $\bar{Q}$  is the non-dimensional bulk humidity, and  $\bar{C}$  is  $C$  rescaled by a factor  $BHU/L$ . A solution for the velocity is sought in the form of asymptotic series  $\mathbf{v} = \mathbf{v}_0 + \varepsilon \mathbf{v}_1 + \dots$ .

As follows from (IIB1), a consistent QG limit  $\varepsilon \rightarrow 0$ , as in the mcRSW model (see Ref. 6), is possible only when the condensation  $\bar{C}$  is small:  $\bar{C} = \mathcal{O}(\varepsilon)$ . Indeed, for the geostrophic velocity, we obtain from (22a) in zeroth order in  $\varepsilon$ ,

$$\hat{z} \wedge \mathbf{v}_0 = -\nabla \eta - \nabla \sigma \equiv -\nabla \psi, \quad (23)$$

where  $\psi = \eta + \sigma$  is the geostrophic streamfunction. Obviously,  $\nabla \cdot \mathbf{v}_0 \equiv 0$ , which is consistent with (22b) only if the RHS is of the order  $\varepsilon$ . Similarly, Eq. (22c) is self-consistent only at  $\bar{C} = \mathcal{O}(\varepsilon)$ . Therefore, in the following, we assume that  $\bar{C} = \varepsilon \hat{C}$  with  $\hat{C} = \mathcal{O}(1)$ .

Let us also recall the standard algorithm for obtaining the QG equations in the “dry” RSW model with  $b = g = \text{const}$  and  $\sigma \equiv 0$ . The first-order divergence is determined from Eq. (22a) in terms of the geostrophic streamfunction

$$\nabla \cdot \mathbf{v}_1 = -\left( \frac{\partial}{\partial t} + \mathbf{v}_0 \cdot \nabla \right) (\nabla^2 \psi)$$

and substituted in (22b) (without the RHS) to give a closed equation for  $\psi$ :

$$\left( \frac{\partial}{\partial t} + \mathbf{v}_0 \cdot \nabla \right) (\nabla^2 \psi - \psi) = 0, \quad (24)$$

with  $\mathbf{v}_0$  given by (23). In the TRSW model, the same procedure gives

$$\nabla \cdot \mathbf{v}_1 = -\left( \frac{\partial}{\partial t} + \mathbf{v}_0 \cdot \nabla \right) \nabla^2 \psi + \mathbf{v}_0 \cdot \nabla \sigma,$$

and instead of (24), we obtain

$$\left( \frac{\partial}{\partial t} + \mathbf{v}_0 \cdot \nabla \right) (\nabla^2 \psi - \psi) - \mathbf{v}_0 \cdot \nabla \sigma = 0,$$

which should be considered together with (22c), with  $\mathbf{v} = \mathbf{v}_0$ . Including condensation leads to the following moist-convective QG-TRSW equations:

$$(\nabla^2 \psi - \psi)_t + \mathcal{J}(\psi, \nabla^2 \psi) - \mathcal{J}(\psi, \sigma) = (1 - \gamma) \hat{C}, \quad (25a)$$

$$\sigma_t + \mathcal{J}(\psi, \sigma) = \frac{\hat{C}}{2}, \quad (25b)$$

$$\hat{Q}_t - \mathcal{J}(\psi, \hat{Q}) + \bar{Q}_s (\nabla^2 \psi_t + \mathcal{J}(\psi, \nabla^2 \psi) - \mathcal{J}(\psi, \sigma)) = \hat{C}, \quad (25c)$$

where  $\mathcal{J}(A, B) := A_x B_y - A_y B_x$  denotes the Jacobian of the pair of functions  $A$  and  $B$  and we have introduced the non-dimensional moisture deficit  $\hat{Q} = Q_s - \bar{Q} = \mathcal{O}(\varepsilon)$  and supposed, for simplicity, that  $Q_s = \text{const}$ , although  $Q_s$  depends, in general, on  $\eta$  (see Ref. 3) and on  $\sigma$  (see below). In the absence of  $\sigma$ , in the limit of immediate relaxation, when  $\hat{Q}$  may be set to zero, Eq. (25c) readily gives the enhancement of the geostrophic relative vorticity  $\nabla^2 \psi$ , that is, enhancement of cyclones and depletion of anticyclones due to condensation, as was noticed in Ref. 6. We see from (25c) that in the moist-convective QG-TRSW, the relationship between the tendency of the relative vorticity and condensation is less direct and is affected by advection of the buoyancy anomaly.

## 2. Charney (weak pressure gradient) limit in the equatorial beta-plane

As is well known (see, e.g., Ref. 17), the geostrophic balance in the equatorial region is not well defined due to the essential dependence of the Coriolis parameter on the meridional coordinate. Nevertheless, an analog of the QG approximation was proposed in the classical paper<sup>18</sup> on the basis of the observation that pressure gradients are small in the tropical atmosphere. The conjecture of small pressure gradients is supported by data analysis.<sup>19</sup> The Charney approach has recently been applied in Ref. 20 to the RSW equations on the equatorial beta-plane. It is based on the assumption that variations of  $h$  are small, which implies the smallness of the Froude number for consistency. In the TRSW model, the smallness of the variations of  $h$  does not automatically imply that the Froude number, which is the ratio of the typical velocity of the flow to the phase velocity of the “dry” thermal gravity waves  $c_d = \sqrt{BH}$  is small. Let us use the same scaling (20) along with the hypothesis of smallness of thickness perturbations, but without additional hypotheses on the (equatorial) Rossby number or smallness of the perturbations of  $b$  and assume that  $Fr := U/c_d = \mathcal{O}(1)$ , that is, that we are dealing with fast equatorial motions. We then obtain from (IIA) considered on the equatorial beta-plane where  $f(y) = \beta y$ , in the leading order in  $\varepsilon$ , which controls the amplitude of thickness perturbations:

$$\mathbf{v}_t + \mathbf{v} \cdot \nabla \mathbf{v} + \tilde{\beta} y \hat{z} \wedge \mathbf{v} + \nabla \bar{b} = 0, \tag{26a}$$

$$\nabla \cdot \mathbf{v} = -\frac{1-\gamma}{\bar{b}} \bar{C}, \tag{26b}$$

$$\bar{b}_t + \mathbf{v} \cdot \nabla \bar{b} = \bar{C}, \tag{26c}$$

$$\bar{Q}_t + \nabla \cdot (\bar{Q} \mathbf{v}) = -\bar{C}. \tag{26d}$$

Here, the non-dimensional gradient of the Coriolis parameter  $\tilde{\beta} := \beta L^2/U$  is the inverse of the equatorial Rossby number and  $\bar{b} := b/B$  is the non-dimensional buoyancy. Notice that Eq. (26a) has the same form as in the RSW model, and following the standard procedure, we obtain the absolute vorticity evolution equation by cross-differentiation,

$$\left( \frac{\partial}{\partial t} + \mathbf{v} \cdot \nabla \right) (\zeta + \tilde{\beta} y) + (\zeta + \tilde{\beta} y) \nabla \cdot \mathbf{v} = 0,$$

where  $\zeta := v_x - u_y$  is the relative vorticity. In view of (26b), this is equivalent to

$$\left( \frac{\partial}{\partial t} + \mathbf{v} \cdot \nabla \right) (\zeta + \tilde{\beta} y) = \frac{(1-\gamma)}{\bar{b}} (\zeta + \tilde{\beta} y) \bar{C}. \tag{27}$$

This equation helps to qualitatively analyze the evolution of vorticity. For example, as is easy to see, it amplifies the cyclones at both sides of the Equator in the condensation regions.

It should be emphasized that Eqs. (26a), (26b), and (26d) resemble the non-dissipative version of the so-called weak temperature gradients model for the dynamics of the equatorial atmosphere; see Ref. 21. However, if the gradients of (potential) temperature are supposed to be small, as in (21), then similar to the analysis of QG regime arguments show that first,  $\bar{C}$  should be of the order  $\varepsilon$ , and second,  $U \ll c_d$  for consistency. In this way, the first three equations in (IIB2) become

$$\mathbf{v}_t + \mathbf{v} \cdot \nabla \mathbf{v} + \tilde{\beta} y \hat{z} \wedge \mathbf{v} + \nabla (\eta + \sigma) = 0, \tag{28a}$$

$$\nabla \cdot \mathbf{v} = 0, \tag{28b}$$

$$\sigma_t + \mathbf{v} \cdot \nabla \sigma = \hat{C}, \tag{28c}$$

while Eq. (26d) giving the evolution of  $\hat{Q}$  requires the knowledge of divergence of the first correction to the velocity, as in the QG regime. Thus, we see that the “weak temperature gradient” model is, in essence, a weak pressure gradient one in the TRSW context, while it is the weak temperature and weak pressure gradient model, which is an analog of the Charney model in the RSW context. It can be shown that, as in the latter one, it admits modon solutions.<sup>20</sup>

## C. Putting flesh on the skeleton

### 1. Parameterizing momentum, water vapor, and heat exchanges with the exterior

The first improvement of the skeleton model consists in adding on the RHS of Eq. (19d), a source of moisture due to evaporation in the boundary layer. The boundary layer itself will not be modeled, and its influence is represented by bulk formulas in the model. For the evaporation, we use

$$E = \alpha |\mathbf{v}| (Q_s - Q) \mathcal{H}(Q_s - Q), \tag{29}$$

where  $\alpha$  is a coefficient that, in general, can depend on the variables of the model. This formula is well adapted for the atmospheric dynamics over the ocean, which is of our primary interest; see below. In order to account for the contrast between the ocean and the continents, the evaporation coefficient could change its value over the land, in a minimalistic approach, or the whole parameterization could be modified there.

Another influence of the boundary layer consists of the momentum and mass exchanges with the main layer, which can, again in a minimalistic way, be accounted for by a bottom friction term,

$$\mathbf{D} = -K(|\mathbf{v}|) \mathbf{v}, \tag{30}$$

on the RHS of Eq. (19a), where  $K$  is typically a linear function. A radiative cooling/heating of the atmosphere is usually represented in shallow water models as a relaxation of  $h$  to an equilibrium profile;

see, e.g., Ref. 22. The TRSW model allows one to do it in a more consistent way by including the radiative relaxation term

$$R = -\frac{1}{\tau_r}(b - b_e), \quad (31)$$

on the RHS of Eq. (19c), where  $b_e(x, y)$  is an equilibrium distribution, which in the simplest case is just a background mean value  $b_e(x, y) \equiv B$ . In the same way, a different, but shorter, relaxation time, can represent the adjustment of the potential temperature of the air to the sea-surface temperature (SST),

$$T = -\frac{1}{\tau_s}(b - b_s), \quad (32)$$

where  $b_s(x, y, t)$  is the buoyancy built with an equivalent potential temperature corresponding to the SST. It should be stressed that a similar parameterization of the heat exchanges was used in oceanographic applications of the TRSW model in Ref. 14. To finish with heat, water vapor, and momentum exchanges, let us mention that, as it was explained in Ref. 10, there is an ambiguity in assigning the Stokes drag resulting from the convective flux from the lower to upper layer in the two-layer model, of which the current one-layer model is a limit of infinitely thick upper layer. The Stokes drag is proportional to the velocity difference between the layers, and in the one-layer limit, with motionless upper layer, the convention adopted in Ref. 3 was that the Stokes drag affects only the upper layer. If the Stokes drag acts also upon the lower layer, a term,

$$\mathbf{S} = -\delta \frac{\mathbf{v}}{h} \beta_1 C, \quad (33)$$

is to be added to the RHS of Eq. (19a), where  $0 \leq \delta \leq 1$  is a coefficient reflecting the aforementioned uncertainty in assigning the Stokes drag.

## 2. Adding new ingredients

In the skeleton version of Sec. II A, the condensed water vapor drops off. Therefore, condensation is equivalent to precipitation, and it was understood in this sense in Ref. 3. However, condensed water remains in the atmosphere in the form of clouds, and precipitation is switched on only when water droplets reach some critical size. Following Ref. 10, we include precipitable water in the model in the form of another advected quantity, with a source due to condensation. Once liquid water is included in the model, we can also include vaporization. A bulk amount of precipitable water  $W(x, y, t)$  in the air column obeys the following equation:

$$W_t + \nabla \cdot (W\mathbf{v}) = C - V, \quad (34)$$

where  $V$  stands for vaporization. Opposite the condensation, vaporization results in cooling and hence produces a downward convective flux. This extra flux gives rise to extra terms in the mass and momentum equations, in the same way as condensation, but with an opposite sign. The vaporization itself can be modeled by a relaxation of  $Q$  toward  $Q_s$  from below, but with coefficient smaller by an order of magnitude, compared to condensation; see Ref. 10. However, in what follows, we are mostly interested in the configuration where  $Q$  is close to saturation and hence will be neglecting the vaporization process. On the contrary, the precipitation is important in such a setting and will be introduced as a sink in (34), again as a relaxation

with a relaxation time  $\tau_p$  to a critical bulk amount of precipitable water in the column, beyond which the precipitation starts,

$$P = \frac{W - W_{cr}}{\tau_p} \mathcal{H}(W - W_{cr}). \quad (35)$$

A phenomenon that could be included in the model to further increase the realism of the representation of the water cycle is the entrainment of liquid water by convective updrafts. This process can be simply modeled as a sink in the precipitable water equation, which is proportional, with some coefficient  $\kappa$ , to the upward convective flux, and hence, to the condensation.

Finally, although we will be using, for simplicity, a constant  $Q_s$  in the examples below, it depends, in principle, on deviations of both the thickness and the potential temperature from their mean values, as was already mentioned above. This dependence follows from the Clausius–Clapeyron equation and, in the simplest form, is given by a linear function.

Gathering all of the above-described additions (except vaporization, as explained), we thus arrive at the system of equations of the full one-layer mcTRSW model as follows:

$$\begin{aligned} \mathbf{v}_t + \mathbf{v} \cdot \nabla \mathbf{v} + f(y)\hat{z} \wedge \mathbf{v} &= -b\nabla h - \frac{h}{2}\nabla b + \mathbf{D} + \mathbf{S}, \\ h_t + \nabla \cdot (h\mathbf{v}) &= -\frac{1-\gamma}{b}C, \\ b_t + \mathbf{v} \cdot \nabla b &= \frac{1}{h}C + R + T, \\ Q_t + \nabla \cdot (Q\mathbf{v}) &= -C + E, \\ W_t + \nabla \cdot (W\mathbf{v}) &= (1 - \kappa)C - P, \end{aligned}$$

where  $\beta_1, \beta_2, \mathbf{D}, \mathbf{S}, R, T, C, E$ , and  $P$  are given by Eqs. (3), (18), (29)–(33), and (35), respectively.

Below we will present two examples of applications of the constructed mcTRSW model. The first example is, at the same time, a benchmark, as it repeats the similar test in the mcRSW model from.<sup>3</sup> It consists of the interaction of a gravity wave packet with a moisture front and generation of convection-coupled waves. The second example is an application of the model to the problem of the relaxation of localized disturbances at the Equator.

## III. EXAMPLES OF APPLICATIONS OF mcTRSW

In the numerical examples below, we will take  $\kappa = 0$  and switch off  $\mathbf{D}, \mathbf{S}, R, T$ , and  $P$ , which will be included in future work. The resulting mcTRSW system, rewritten in terms of the conservative variables ( $h$ , zonal momentum density  $\mathcal{Q} := hu$ , meridional momentum density  $\mathcal{P} := hv$ , bulk buoyancy  $\mathcal{B} := hb$ , bulk humidity  $Q$ , and bulk precipitable water  $W$ ) reads as

$$h_t + \mathcal{Q}_x + \mathcal{P}_y = -\frac{1-\gamma}{b}C, \quad (36a)$$

$$\mathcal{Q}_t + \left( \frac{\mathcal{Q}^2}{h} + \frac{h\mathcal{B}}{2} \right)_x + \left( \frac{\mathcal{Q}\mathcal{P}}{h} \right)_y = f\mathcal{P}, \quad (36b)$$

$$\mathcal{P}_t + \left(\frac{\mathcal{Q}\mathcal{P}}{h}\right)_x + \left(\frac{\mathcal{P}^2}{h} + \frac{h\mathcal{B}}{2}\right)_y = -f\mathcal{Q}, \quad (36c)$$

$$\mathcal{B}_t + \left(\frac{\mathcal{B}\mathcal{Q}}{h}\right)_x + \left(\frac{\mathcal{B}\mathcal{P}}{h}\right)_y = \gamma C, \quad (36d)$$

$$Q_t + \left(\frac{Q\mathcal{Q}}{h}\right)_x + \left(\frac{Q\mathcal{P}}{h}\right)_y = -C + E, \quad (36e)$$

$$W_t + \left(\frac{W\mathcal{Q}}{h}\right)_x + \left(\frac{W\mathcal{P}}{h}\right)_y = C. \quad (36f)$$

Unless otherwise stated explicitly,  $\gamma$  is taken to be zero.

For numerical simulations, we use a new well-balanced central-upwind scheme we have recently proposed in Refs. 23 and 24 for the 1-D and two-dimensional (2-D) TRSW equations, respectively. A brief description of the 2-D scheme and of the numerical treatment of the relaxation source terms is presented in the Appendix.

### A. One-dimensional convection-coupled gravity waves

As the first test of the mcTRSW model, we consider the scattering of the packet of gravity waves by a moisture front. The setup is 1-D; that is, there is no dependence on  $x$ , and the rotation, precipitation and evaporation are switched off,

$$\begin{aligned} h_t + \mathcal{P}_y &= -\frac{1-\gamma}{b} C, \\ \mathcal{P}_t + \left(\frac{\mathcal{P}^2}{h} + \frac{h\mathcal{B}}{2}\right)_y &= 0, \\ \mathcal{B}_t + \left(\frac{\mathcal{B}\mathcal{P}}{h}\right)_y &= \gamma C, \\ Q_t + \left(\frac{Q\mathcal{P}}{h}\right)_y &= -C, \\ W_t + \left(\frac{W\mathcal{P}}{h}\right)_y &= C. \end{aligned}$$

We take the same initial conditions as in Experiment 1 of Ref. 3, albeit with the lower value of the saturation threshold, in order to let the wave cross the front. The moisture front is taken to have the following form:

$$Q(y, 0) = Q_c [1 + 0.05 \tanh((y - y_M)\mathcal{H}(y + y_M))],$$

where  $y_M = 6$  is the middle of the computational domain  $[0, 12]$ , in which we introduce a uniform mesh with 1500 finite-volume cells, and  $Q_c = 0.89$ . Initial  $b$  and  $W$  are constant:  $b(y, 0) \equiv 1$  and  $W(y, 0) \equiv 0$ . Since the precipitation is switched off,  $W$ , when it appears, signals condensation “clouds.” The initial wave-packet was placed on the left of the front, in the “dry” zone, and was chosen in a way that it was moving toward the moisture front:

$$v(y, 0) = \mu(y), \quad h(y, 0) = 1 + \mu(y),$$

where

$$\mu(y) = [-(y - y_P)^2 + \varepsilon] \mathcal{H}(y - y_P + \sqrt{\varepsilon}) \mathcal{H}(-y + y_P + \sqrt{\varepsilon}).$$

Here,  $y_P = 2$  is an initial position of the wave-packet of a parabolic form and  $\varepsilon = 0.025$  determines both the amplitude and width of the packet. The parameters used in (3) and (29) are  $Q_c = 0.9$  and  $\tau = 0.02$ .

The results of the simulations are fully consistent with those of Ref. 3, apart from the fact that due to a lower  $Q_c$ , the packet now penetrates into the “moist” zone to the right of the front and propagates as a convection-coupled wave. In the upper row of Fig. 2, we present the time evolution of thickness and velocity. They clearly show a partial reflection from, and as a penetration into the “moist” zone by the wave-packet.

Yet, compared to Ref. 3, we have new elements: diabatic heating resulting in a local increase of  $b$ , and a “cloud” formation related to the condensed water  $W$ . Both are well represented by the scheme, as follows from Fig. 2 (lower row), where we show the snapshots of the evolution of  $b$ , and Fig. 3, where we display the Hovmöller (characteristic) diagram for  $W$ . As follows from these figures, the initially constant  $b$  increases locally when the wave-packet hits the moisture front and condensation starts. The increase in  $b$  then spreads rightwards, following the propagating wave. Condensed water  $W$  starts forming at the same moment and then follows the wave, the “clouds” never disappearing as the precipitation and vaporization are switched off.

### B. Equatorial adjustment of localized pressure and potential temperature anomalies

As the second example of applications of the mcTRSW model, we consider the relaxation of localized perturbations of pressure and temperature at the Equator, the equatorial adjustment.<sup>25</sup> The motivation for considering this example is twofold. First, starting from the pioneering works,<sup>2,26</sup> the rotating shallow water model has become a classical tool in understanding the circulation of the tropical atmosphere. Yet, the heating due to moist convection was understood as a source/sink in the equation for  $h$  in the classical works<sup>5,26</sup> and subsequent papers; see Refs. 21 and 27. The TRSW model allows one to distinguish between the mass source/sink and heating/cooling (potential temperature source/sink), and it is interesting to compare their respective effects. Second, it is well known that, overall, the temperature gradients in the equatorial region are weak (see, e.g., Ref. 21), which makes this region well suited for applications of the TRSW equations. Let us recall that a given velocity profile of, for example, a jet or a vortex, can be maintained in the TRSW model by pressure gradients (geostrophic or cyclo-geostrophic balance), density/temperature gradients (thermal balance), or a combination of both thermo- and cyclo-geostrophic balance;<sup>28</sup> see (23). It was shown that purely thermal, or thermally dominated, that is, with the density/temperature gradients stronger than the pressure gradients, vortices<sup>28</sup> and jets<sup>29,30</sup> (also see Ref. 1, Chap. 14) are subject to specific convective-type instabilities. The interpretation and relevance of these instabilities in the TRSW equations is still to be clarified, but in any case, they typically do not occur if the model is applied to the equatorial atmosphere with realistic parameters, where temperature gradients are generally small. At the same time, the advantage of the TRSW model compared to the RSW



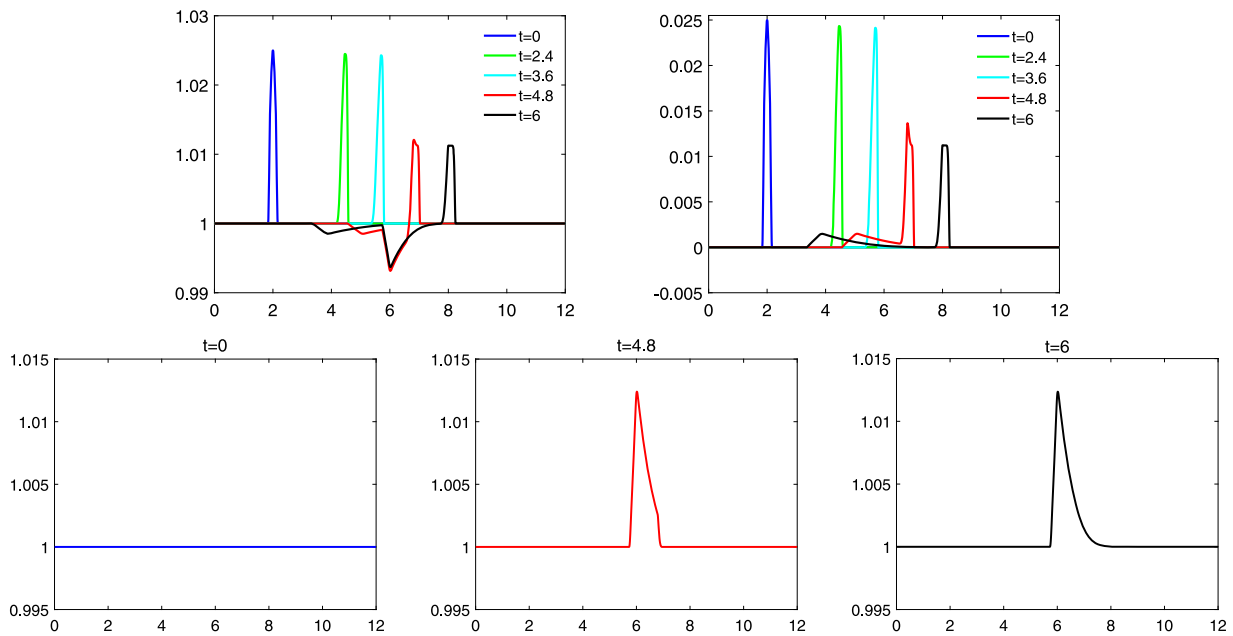


**FIG. 2.** Upper row: Snapshots of the thickness  $h(y, t)$  (left) and velocity  $v(y, t)$  (right) at times  $t = 0, 2.4, 3.6, 4.8,$  and  $6$ . Lower row: Snapshots of the buoyancy  $b(y, t)$  at times  $t = 0, 4.8,$  and  $6$ .

one is that it allows us to track the evolution of (potential) temperature, its changes due to various heat fluxes, and its dynamical influence.

The equatorial adjustment process is directly related to the classical Gill mechanism of the response of the tropical atmosphere to a localized heating.<sup>26,31</sup> The heating in these papers was assimilated to a permanently acting localized forcing term in the equation for  $h$ . Knowing the response to a localized *initial*  $h$  allows us to anticipate

the response in the forced problem, as forcing can be thought of as permanently recreating the localized perturbation of  $h$ .

We start by benchmarking the model on the equatorial beta-plane with non-dimensional  $f(y) = y$  in the “dry” configuration, that is, we numerically solve the system

$$\begin{aligned} h_t + \mathcal{Q}_x + \mathcal{P}_y &= 0, \\ \mathcal{Q}_t + \left(\frac{\mathcal{Q}^2}{h} + \frac{h\mathcal{B}}{2}\right)_x + \left(\frac{\mathcal{Q}\mathcal{P}}{h}\right)_y &= f\mathcal{P}, \\ \mathcal{P}_t + \left(\frac{\mathcal{Q}\mathcal{P}}{h}\right)_x + \left(\frac{\mathcal{P}^2}{h} + \frac{h\mathcal{B}}{2}\right)_y &= -f\mathcal{Q}, \\ \mathcal{B}_t + \left(\frac{\mathcal{B}\mathcal{Q}}{h}\right)_x + \left(\frac{\mathcal{B}\mathcal{P}}{h}\right)_y &= 0, \end{aligned}$$

starting with the initial conditions close to those used in the numerical simulations with the RSW model on the equatorial beta-plane in Ref. 25, that is,

$$\begin{aligned} u(x, y, 0) = v(x, y, 0) &\equiv 0, & b(x, y, 0) &\equiv 1, \\ h(x, y, 0) &= 1 - \varepsilon e^{-\left(\frac{x^2}{2a^2} + \frac{y^2}{2}\right)}, \end{aligned} \tag{37}$$

where  $\varepsilon$  is the non-dimensional amplitude of the initial perturbation and  $a$  is its aspect ratio. We have used  $\varepsilon = 0.2$  and  $a = 5$  so as to be consistent with the long-wave scaling used in Refs. 5 and 31 and in the theoretical analysis of Ref. 25. The numerical simulations

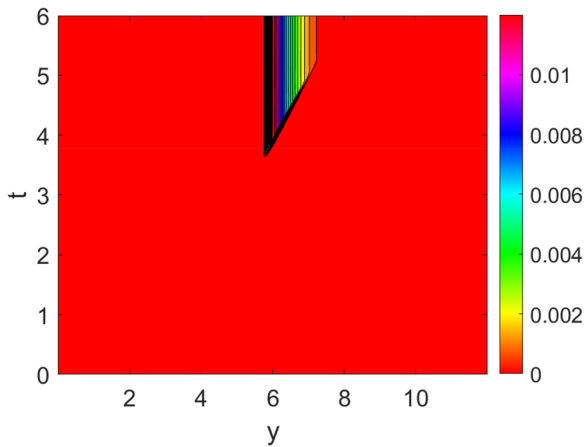


**FIG. 3.** Hovmöller diagram for  $W(y, t)$ .

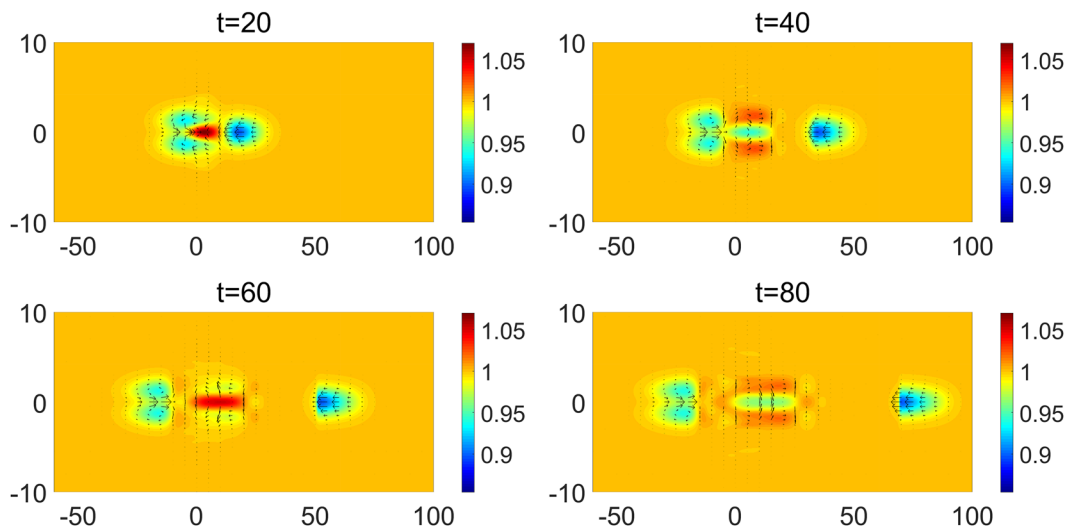


FIG. 4. Snapshots of  $h$  (colors) and velocity (arrows) fields during the “dry” equatorial adjustment of zonally elongated negative anomaly of  $h$  at times  $t = 20, 40, 60,$  and  $80$ .

are performed in the domain  $[-100, 100] \times [-10, 10]$  using a  $1000 \times 1000$  uniform mesh. The evolution of  $h$  and velocity, shown in Fig. 4, is fully consistent with that of Ref. 25: the initial disturbance generates a Kelvin wave rapidly moving to the right (eastward), and steepening at the rear, as it is a depression Kelvin wave, a Rossby wave packet with dipolar structure, which is symmetric with respect to the Equator, slowly moving to the left (westward) and a stagnant inertia-gravity wave packet at the location of the initial perturbation.

We then solve system (III) with  $Q_s = 0.7, \tau = 0.15, \alpha = 0.1,$  and the initial conditions (37) together with

$$Q(x, y, 0) \equiv Q_s - 0.01, \quad W(x, y, 0) \equiv 0. \quad (38)$$

The evolution of  $h$  and velocity is presented in Fig. 5. Although similar, Figs. 4 and 5 show significant differences. The pressure minima in the Kelvin wave and in the Rossby wave are more pronounced in the moist case, and there remains a quasi-permanent

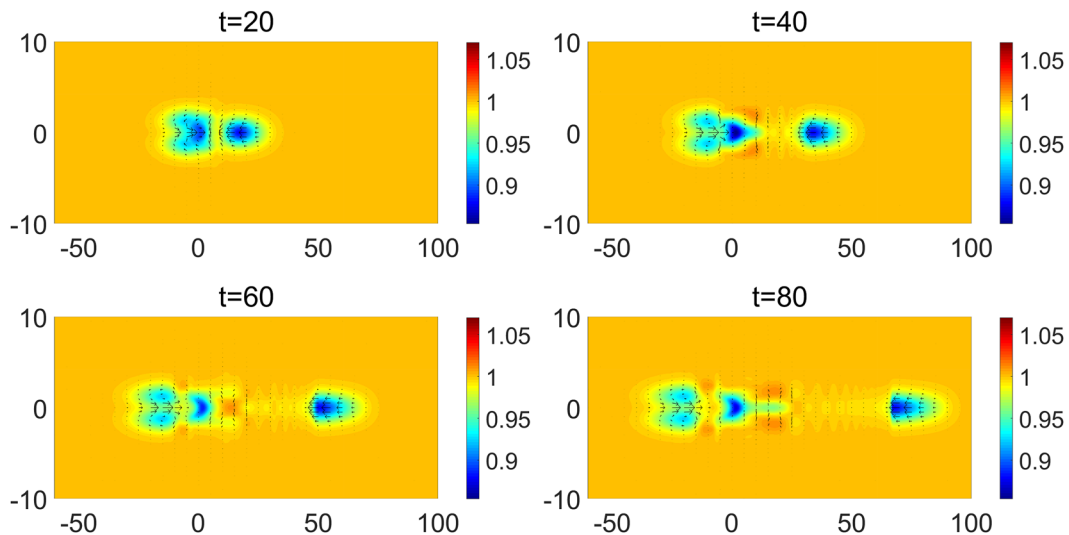


FIG. 5. Same as in Fig. 4, but for “moist-convective” equatorial adjustment.

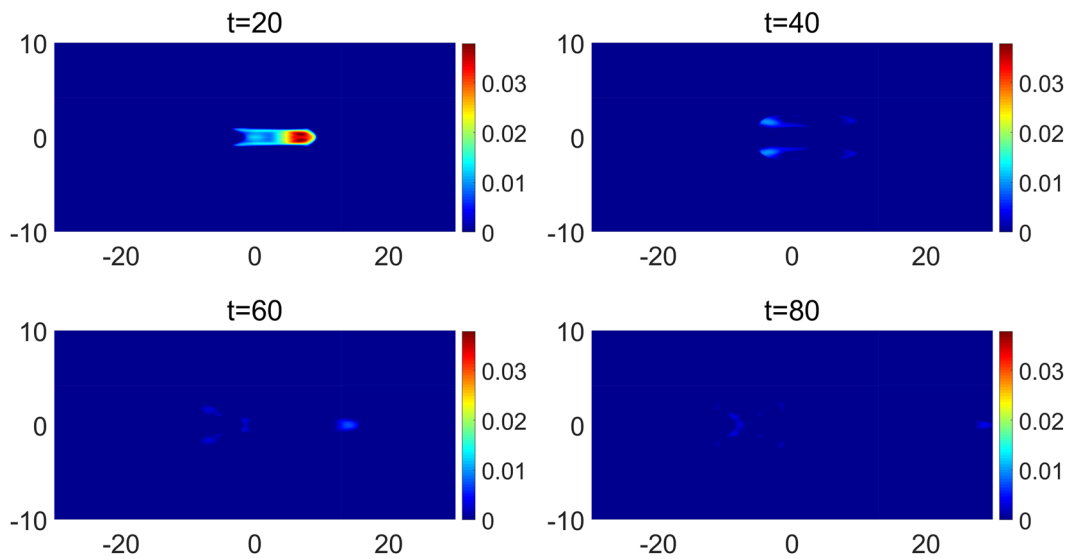


FIG. 6. Same as in Fig. 5, but for the condensation  $C$ .

depression at the initial location. Both effects are due to the condensation, which is displayed in Fig. 6. Notice that while the Kelvin wave drops out in the leading order under the Charney scaling of Sec. II B 2, the Rossby waves remain, and their intensification is consistent with (27). The condensation also produces a localized heating, which creates a persisting buoyancy anomaly, as can be seen in Fig. 7.

In order to compare the adjustment of localized pressure and (potential) temperature perturbations, we perform simulations with

the same initial conditions, but with  $b$  and  $h$  interchanged in (37), that is, with flat  $h$  and Gaussian  $b$ . The corresponding evolution of  $h$  with the velocity and  $b$  is presented in Figs. 8 and 9, respectively. A comparison of the zonal cross sections of thickness along the Equator,  $h(x, 0, 80)$ , corresponding to the snapshots at time  $t = 80$  from Figs. 4, 5, and 8 are presented in Fig. 10. As one can see, the evolution of  $h$  is qualitatively similar to both “dry” and “moist-convective” adjustments of the pressure anomaly of the same form and amplitude in the Kelvin- and Rossby-wave sectors, while the

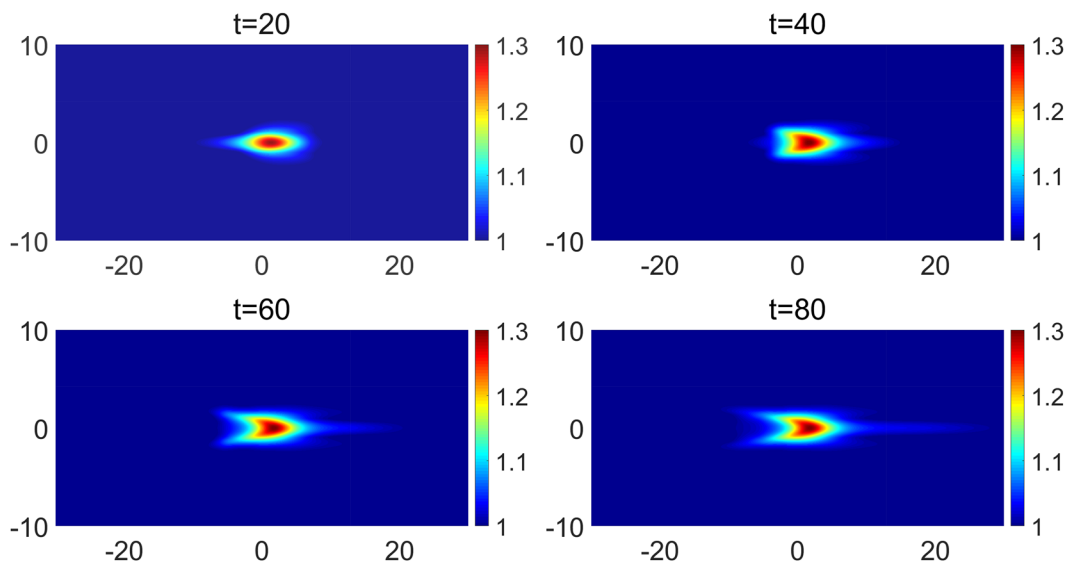


FIG. 7. Same as in Fig. 5, but for the buoyancy  $b$ .

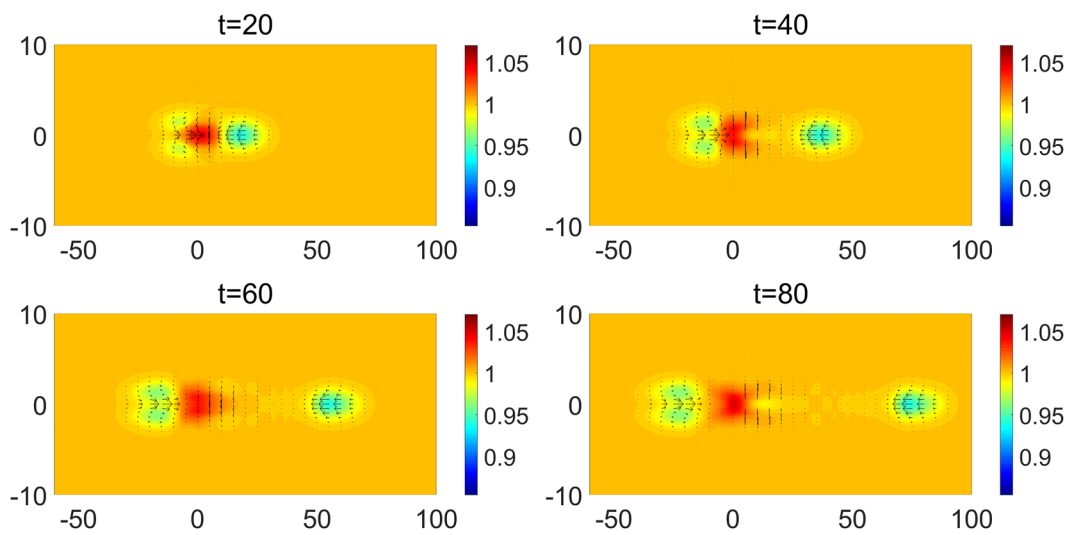


FIG. 8. Same as in Fig. 5, but for initially flat  $h$  and Gaussian  $b$ .

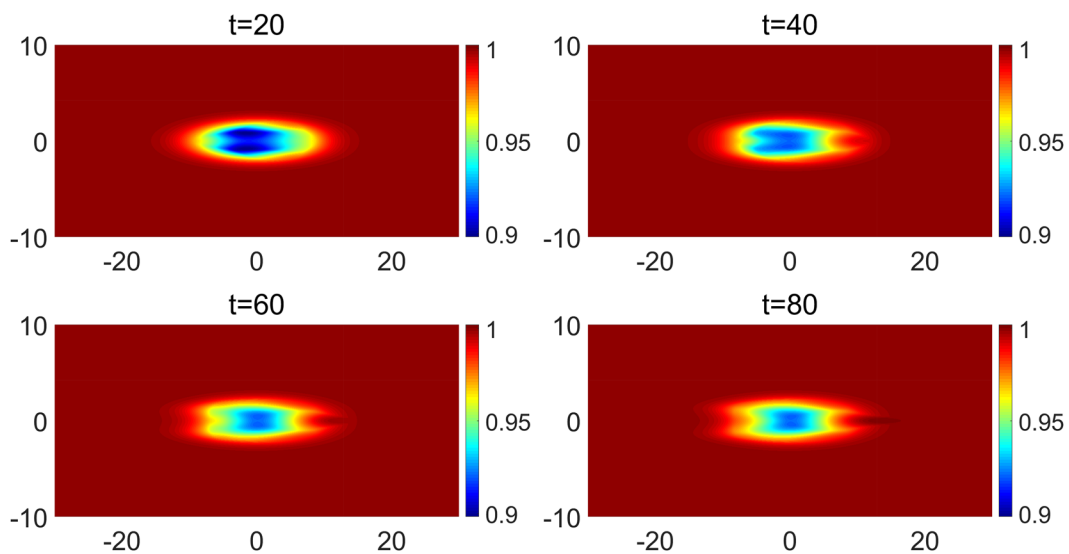


FIG. 9. Same as in Fig. 8, but for the buoyancy  $b$ .

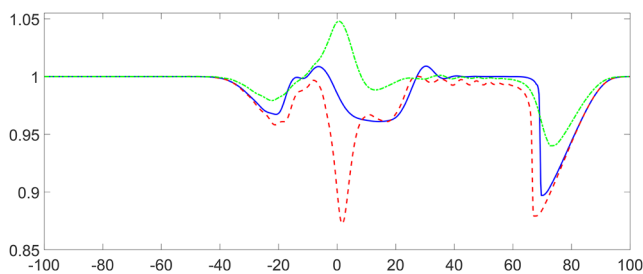
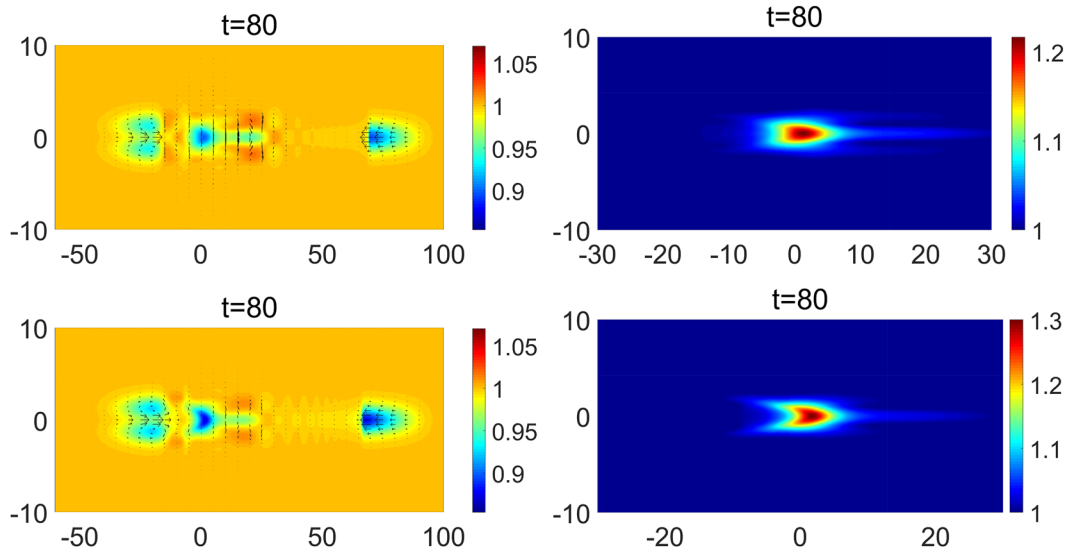


FIG. 10. Zonal profiles of thickness at the Equator,  $h(x, 0)$ , at  $t = 80$  from the simulations of Fig. 4 (continuous line), 5 (dashed line), and 8 (dashed-dotted line).

activity at the location of initial perturbation is totally different. Figure 9 shows that the evolution of buoyancy is different, as the initial negative anomaly is modified by the heating due to the condensation. This latter evolves, qualitatively, as in Fig. 6, but is much weaker (not shown).

Let us finally comment on the changes in the results with the change of the value of parameter  $\gamma$ . Instead of taking  $\gamma = 0$ , we now consider  $\gamma = 0.45$  and the initial data given by (37) and (38). The results remain qualitatively the same, but we do observe certain changes, as one can see in Fig. 11. Since there is no *a priori* preferred value of  $\gamma$ , an additional information is needed to fix it when modeling a given process.



**FIG. 11.** Snapshots of  $h$  (colors) and velocity (arrows) fields (left) and  $b$  (right) at  $t = 80(\beta R_e)^{-1}$  for a simulation with  $\gamma = 0.45$  (upper row) as compared with the solutions at the same time presented in Figs. 5 and 7 (lower row) for  $\gamma = 0$ .

#### IV. SUMMARY AND DISCUSSION

The main purpose of the present paper was to introduce, in a systematic way, the effects of moist convection in the thermal rotating shallow water model along the lines announced in Ref. 3 and study the resulting mcTRSW model numerically using a robust finite-volume scheme. As we have shown, the proposed model is self-consistent and also has consistent and physically reasonable asymptotic limits. The presented numerical examples show that the mcTRSW model reproduces well the convection-coupled gravity and equatorial waves and is ready for a future, more extensive, use. The main advantage of this version of the shallow water model with moist convection over the mcRSW equations, which already proved to be useful, is a possibility of coupling the new model in a very simple, albeit systematic, way with the ocean via the relaxation to the SST, which opens a range of new possibilities. The next step is an extension of the model to two or three layers in order to include the effects of baroclinicity. This work is in progress.

The mcTRSW model not only allows for a simplified but self-consistent modeling of complex atmospheric phenomena, but can also be used for testing the general circulation models (GCM), if considered in the spherical geometry as well as data assimilation schemes. In this context, we should mention that the TRSW model was recently rediscovered yet another time in Ref. 32 by vertical averaging of the Boussinesq equations in geometric coordinates and using the absolute temperature as the thermodynamic variable. It was supplied by a realistic precipitation scheme borrowed from the atmospheric general circulation models, apparently without the knowledge of the previous work,<sup>3</sup> and successfully tested. Although we prefer to limit ourselves by the most crude, simple, robust, and numerically friendly parameterizations of condensation, moist convection, and precipitation, this example shows that more elaborate parameterizations of these phenomena are also possible within the

model. It should be pointed out that the advantage of our numerical scheme with respect to the existing schemes for the TRSW model is that it correctly resolves sharp fronts, which are ubiquitous, as we have shown, and also maintains the equilibrium states. However, its spherical version is not available yet.

#### ACKNOWLEDGMENTS

The work of A.K. was supported in part by NSFC Grant No. 11771201 and by the funding of the Guangdong Provincial Key Laboratory of Computational Science and Material Design (Grant No. 2019B030301001). The work of A.K. and V.Z. was supported in part by the French National Program LEFE-MANU.

#### APPENDIX: A SKETCH OF THE NUMERICAL SCHEME

We briefly describe here the 2-D well-balanced central-upwind scheme that was used in the numerical simulations presented in Sec. III, to numerically solve the mcTRSW system (III).

In order to design a well-balanced central-upwind scheme for (III), we follow Ref. 24 (also see Refs. 23 and 33–35) and use the flux globalization approach by incorporating the Coriolis forces into the following two global fluxes:

$$\begin{aligned}\mathcal{K} &= \frac{\mathcal{Q}^2}{h} + \frac{h\mathcal{B}}{2} - \int^x f(y) \mathcal{P}(\xi, y) d\xi, \\ \mathcal{L} &= \frac{\mathcal{P}^2}{h} + \frac{h\mathcal{B}}{2} + \int^y f(\eta) \mathcal{Q}(x, \eta) d\eta.\end{aligned}\quad (\text{A1})$$

The system of balance laws (III) can be recast in the vector form as follows:

$$\mathbf{U}_t + \mathbf{F}(\mathbf{U}, \mathcal{K})_x + \mathbf{G}(\mathbf{U}, \mathcal{L})_y = \mathbf{N}(\mathbf{U}), \quad (\text{A2})$$

where

$$\begin{aligned}
 \mathbf{U} &:= (h, \mathcal{Q}, \mathcal{P}, \mathcal{B}, Q, W)^\top, \\
 \mathbf{F}(\mathbf{U}, \mathcal{X}) &:= \left( \mathcal{Q}, \mathcal{X}, \frac{\mathcal{Q}\mathcal{P}}{h}, \frac{\mathcal{B}\mathcal{Q}}{h}, \frac{Q\mathcal{Q}}{h}, \frac{W\mathcal{Q}}{h} \right)^\top, \\
 \mathbf{G}(\mathbf{U}, \mathcal{L}) &:= \left( \mathcal{P}, \frac{\mathcal{Q}\mathcal{P}}{h}, \mathcal{L}, \frac{\mathcal{B}\mathcal{P}}{h}, \frac{Q\mathcal{P}}{h}, \frac{W\mathcal{P}}{h} \right)^\top, \\
 \mathbf{N} &:= \left( -\frac{1-\gamma}{\mathcal{B}} hC, 0, 0, \gamma C, -C + E, C \right)^\top.
 \end{aligned} \tag{A3}$$

We then apply the semi-discrete Riemann-problem-solver-free central-upwind scheme to (A1)–(A3),

$$\begin{aligned}
 \frac{d}{dt} \bar{\mathbf{U}}_{j,k}(t) &= - \frac{\mathcal{F}_{j+\frac{1}{2},k}(t) - \mathcal{F}_{j-\frac{1}{2},k}(t)}{\Delta x} \\
 &\quad - \frac{\mathcal{G}_{j,k+\frac{1}{2}}(t) - \mathcal{G}_{j,k-\frac{1}{2}}(t)}{\Delta y} + \mathcal{N}_{j,k}(t),
 \end{aligned}$$

where  $I_{j,k} := [x_{j-\frac{1}{2}}, x_{j+\frac{1}{2}}] \times [y_{k-\frac{1}{2}}, y_{k+\frac{1}{2}}]$  are the finite-volume cells of size  $|I_{j,k}| = \Delta x \Delta y$ ,  $\bar{\mathbf{U}}_{j,k}(t) \approx \frac{1}{|I_{j,k}|} \iint_{I_{j,k}} \mathbf{U}(x, y, t) dx dy$  are the computed cell averages  $\mathcal{F}_{j+\frac{1}{2},k}(t)$  and  $\mathcal{G}_{j,k+\frac{1}{2}}(t)$  are the central-upwind fluxes (developed in Refs. 24 and 36), computed using the reconstructed point values of  $\mathbf{U}$  at the middle points of the corresponding cell sides:  $(x_{j+\frac{1}{2}}, k)$  and  $(x_j, y_{k+\frac{1}{2}})$ , and  $\mathcal{N}_{j,k}(t) \approx \frac{1}{|I_{j,k}|} \iint_{I_{j,k}} \mathbf{N}(\mathbf{U}(x, y, t)) dx dy$ .

The scheme is second order accurate provided the point values are reconstructed using a piecewise linear approximation. In order to ensure that the proposed scheme is well-balanced (in the sense that it is capable of preserving certain QG equilibria), we use special well-balanced reconstruction and evolution techniques. More specifically, instead of reconstructing the conservative variables  $\mathbf{U}$ , we reconstruct the equilibrium variables  $\mathcal{Q}, \mathcal{P}, \mathcal{B}, \mathcal{X}$  (in the  $x$ -direction),  $\mathcal{L}$  (in the  $y$ -direction),  $Q$ , and  $W$  to ensure that the reconstruction is well-balanced; see Ref. 24 for details. In addition, we use a numerical diffusion switch function to slightly modify the original central-upwind numerical fluxes from Ref. 36 to guarantee the well-balanced property of the evolution step; see Ref. 24 for details.

Notice that if the condensation ( $C$ ) and evaporation ( $E$ ) are neglected, then system (36a)–(36d) reduces to the TRSW model, for which the central-upwind scheme has been developed in Ref. 24. The extension to the studied system (III) is quite straightforward. First, the left-hand sides of Eqs. (36e) and (36f) have a similar form to the left-hand side of Eq. (36a), and thus they can be treated similarly. Second, the source terms are approximated using the midpoint quadrature as follows:

$$\mathcal{N}_{j,k} = \left( -\frac{1-\gamma}{\mathcal{B}_{j,k}} \bar{h}_{j,k} C_{j,k}, 0, 0, \gamma C_{j,k}, -C_{j,k} + E_{j,k}, C_{j,k} \right)^\top,$$

where

$$C_{j,k} = \frac{\bar{Q}_{j,k} - Q_s}{\tau} \mathcal{H}(\bar{Q}_{j,k} - Q_s)$$

and

$$E_{j,k} = \frac{\alpha}{h_{j,k}} \sqrt{\mathcal{Q}_{j,k}^2 + \mathcal{P}_{j,k}^2} (Q_s - \bar{Q}_{j,k}) \mathcal{H}(Q_s - \bar{Q}_{j,k}).$$

## DATA AVAILABILITY

The data that support the findings of this study are available from the corresponding author upon reasonable request.

## REFERENCES

- V. Zeitlin, *Geophysical Fluid Dynamics: Understanding (almost) Everything with Rotating Shallow Water Models* (Oxford University Press, Oxford, 2018), p. xix+488.
- T. Matsuno, “Quasi-geostrophic motions in the equatorial area,” *J. Meteorol. Soc. Jpn.* **44**, 25–43 (1966).
- F. Bouchut, J. Lambaerts, G. Lapeyre, and V. Zeitlin, “Fronts and nonlinear waves in a simplified shallow-water model of the atmosphere with moisture and convection,” *Phys. Fluids* **21**, 116604 (2009).
- J. Lambaerts, G. Lapeyre, V. Zeitlin, and F. Bouchut, “Simplified two-layer models of precipitating atmosphere and their properties,” *Phys. Fluids* **23**, 046603 (2011).
- A. E. Gill, “Studies of moisture effects in simple atmospheric models: The stable case,” *Geophys. Astrophys. Fluid Dyn.* **19**, 119 (1982).
- J. Lambaerts, G. Lapeyre, and V. Zeitlin, “Moist versus dry barotropic instability in a shallow water model of the atmosphere with moist convection,” *J. Atmos. Sci.* **68**, 1234–1252 (2011).
- J. Lambaerts, G. Lapeyre, and V. Zeitlin, “Moist versus dry baroclinic instability in a simplified two-layer atmospheric model with condensation and latent heat release,” *J. Atmos. Sci.* **69**, 1405–1426 (2012).
- M. Rostami and V. Zeitlin, “Influence of condensation and latent heat release upon barotropic and baroclinic instabilities of atmospheric vortices in a rotating shallow water model on the  $f$ -plane,” *Geophys. Astrophys. Fluid Dyn.* **111**, 1–31 (2017).
- N. Lahaye and V. Zeitlin, “Understanding instabilities of tropical cyclones and their evolution with a moist convective rotating shallow-water model,” *J. Atmos. Sci.* **73**, 505–523 (2016).
- M. Rostami and V. Zeitlin, “Improved moist-convective rotating shallow water model and its application to instabilities of hurricane-like vortices,” *Q. J. R. Meteorol. Soc.* **144**, 1450–1462 (2018).
- E. S. Warnford and P. J. Dellar, “The quasi-geostrophic theory of the thermal shallow water equations,” *J. Fluid Mech.* **723**, 374–403 (2013).
- R. L. Lavoie, “A mesoscale numerical model of lake-effect storms,” *J. Atmos. Sci.* **29**, 1025–1040 (1972).
- M. L. Salby, “Deep circulations under simple classes of stratification,” *Tellus A* **41A**, 48–65 (1989).
- J. P. McCreary, H. S. Lee, and D. B. Enfield, “The response of the coastal ocean to strong offshore winds: With application to circulations in the Gulfs of Tehuantepec and Papagayo,” *J. Marine Res.* **47**, 81–109 (1989).
- W. R. Young, “The subinertial mixed layer approximation,” *J. Phys. Oceanogr.* **24**, 1812–1826 (1994).
- P. Ripa, “On improving a one-layer ocean model with thermodynamics,” *J. Fluid Mech.* **303**, 169–201 (1995).
- I. N. James, *Introduction to Circulating Atmospheres* (Cambridge University Press, 1994).
- J. G. Charney, “A note on large-scale motions in the tropics,” *J. Atmos. Sci.* **20**, 607–609 (1963).
- J.-I. Yano, S. Mulet, and M. Bonazzola, “Tropical large-scale circulations: Asymptotically non-divergent?,” *Tellus A* **61A**, 417–427 (2009).
- M. Rostami and V. Zeitlin, “Eastward-moving convection-enhanced motions in shallow water in the equatorial tangent plane,” *Phys. Fluids* **31**, 021701 (2019).
- A. H. Sobel, J. Nilsson, and L. M. Polvani, “The weak temperature gradient approximation and balanced tropical moisture waves,” *J. Atmos. Sci.* **58**, 3650–3665 (2001).
- W. J. M. Seviour, D. W. Waugh, and R. K. Scott, “The stability of Mars annular polar vortex,” *J. Atmos. Sci.* **74**, 1533–1547 (2017).

- <sup>23</sup>A. Kurganov, Y. Liu, and V. Zeitlin, “A well-balanced central-upwind scheme for the thermal rotating shallow water equations,” *J. Comput. Phys.* **411**, 109414 (2020).
- <sup>24</sup>A. Kurganov, Y. Liu, and V. Zeitlin, “Thermal vs isothermal rotating shallow water equations: Comparison of dynamical processes by simulations with a novel well-balanced central-upwind scheme” *Geophys. Astrophys. Fluid Dyn.* (submitted) (2020), available at <https://sites.google.com/view/alexander-kurganov/publications>.
- <sup>25</sup>J. L. Sommer, G. M. Reznik, and V. Zeitlin, “Nonlinear geostrophic adjustment of long-wave disturbances in the shallow-water model on the equatorial beta-plane,” *J. Fluid Mech.* **515**, 135–170 (2004).
- <sup>26</sup>A. E. Gill, “Some simple solutions for heat induced tropical circulation,” *Q. J. R. Meteorol. Soc.* **106**, 447–462 (1980).
- <sup>27</sup>R. N. Ferreira, W. H. Schubert, and J. J. Hack, “Dynamical aspects of twin tropical cyclones associated with the Madden-Julian oscillation,” *J. Atmos. Sci.* **53**, 929–945 (1996).
- <sup>28</sup>É. Gouzien, N. Lahaye, V. Zeitlin, and T. Dubos, “Thermal instability in rotating shallow water with horizontal temperature/density gradients,” *Phys. Fluids* **29**, 101702 (2017).
- <sup>29</sup>J. P. McCreary, P. K. Kundu, and R. L. Molinari, “A numerical investigation of dynamics, thermodynamics and mixed-layer processes in the Indian Ocean,” *Prog. Oceanogr.* **31**, 181–244 (1993).
- <sup>30</sup>W. R. Young and L. Chen, “Baroclinic instability and thermohaline alignment in the mixed layer,” *J. Phys. Oceanogr.* **25**, 3172–3185 (1995).
- <sup>31</sup>W. A. Heckley and A. E. Gill, “Some simple analytical solutions to the problem of forced equatorial long waves,” *Q. J. R. Meteorol. Soc.* **110**, 203–217 (1984).
- <sup>32</sup>M. Zerroukat and T. Allen, “A moist Boussinesq shallow water equations set for testing atmospheric models,” *J. Comput. Phys.* **290**, 55–72 (2015).
- <sup>33</sup>A. Chertock, M. Herty, and Ş. N. Özcan, “Well-balanced central-upwind schemes for  $2 < \text{mspacewidth} = "0.167em" > \times < \text{mspacewidth} = "0.167em" > 2$  systems of balance laws,” in *Theory, Numerics and Applications of Hyperbolic Problems I*, Springer Proceedings in Mathematics and Statistics Vol. 236 (Springer, 2018), pp. 345–361.
- <sup>34</sup>Y. Cheng, A. Chertock, M. Herty, A. Kurganov, and T. Wu, “A new approach for designing moving-water equilibria preserving schemes for the shallow water equations,” *J. Sci. Comput.* **80**, 538–554 (2019).
- <sup>35</sup>A. Chertock, S. Cui, A. Kurganov, Ş. N. Özcan, and E. Tadmor, “Well-balanced schemes for the Euler equations with gravitation: Conservative formulation using global fluxes,” *J. Comput. Phys.* **358**, 36–52 (2018).
- <sup>36</sup>A. Kurganov and C.-T. Lin, “On the reduction of numerical dissipation in central-upwind schemes,” *Commun. Comput. Phys.* **2**, 141–163 (2007).